THE JOURNAL OF PHYSICAL CHEMISTRY C

Article

pubs.acs.org/JPCC

High Stability and Reactivity of Pt-Based Core−Shell Nanoparticles for Oxygen Reduction Reaction

Zongxian Yang,[†,*] Yanxing Zhang,[†] and Ruqian Wu[‡,*]

[†]College of Physics and Information Engineering, Henan Normal University, Xinxiang, Henan, 453007, People's Republic of China

[‡]Department of Physics and Astronomy, University of California, Irvine, California 92697-4575, United States

ABSTRACT: Structural stability and catalytic reactivity of M@Pt12 core−shell nanoclusters with different core atom (M) are systematically investigated using ab initio density functional theory calculations with the generalized gradient approximation. We found that the pure D_{5h}-Pt13 cluster is venerable to reactants and may loss its activity in reaction conditions. The insertion of Fe, Co, Tc, Ru, Rh, Re, Os, or Ir into its core, forming D_{5h} M@Pt12 core−shell nanoclusters, may significantly enhance the structural stability and may also further improve its catalytic activity. Our findings provide useful insights for the design of robust bimetallic nanocatalysts.

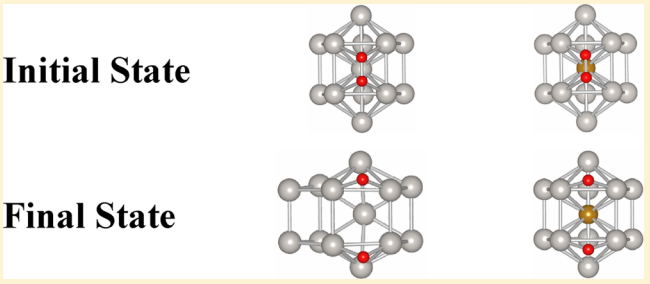

1. INTRODUCTION

Low-temperature fuel cells (FCs) have attracted considerable research interest as a means of producing electricity through direct electrochemical conversion of hydrogen and oxygen into water.[1] Current catalysts on anodes and cathodes are mainly made of platinum, which makes fuel cells very expensive. Moreover, even the best commercial platinum cathodes have a high overpotential due to slow oxygen reduction kinetics resulting in roughly 30% energy loss.[2] Cheaper and more effective electrocatalysts are therefore needed for the further development of fuel cell technology. To this end, bimetallic nanoparticles appear to be potential candidates as platinum alternatives and extensive experimental and theoretical studies for free and supported NPs were extremely active and rewarding in the past decade.[3]

Nanoparticles have high surface-to-volume ratios and exhibit strikingly higher reactivity than their flat surfaces due to the change in chemical bonding and also to the quantum confinement effect. Recent studies attribute the origin of excellent catalytic performance of NPs to the fact that they actually have smaller dimensions than previously anticipated.[4−6] Kaden et al. reported that Pd20 (i.e., consisting of 20 Pd atoms) nanoclusters supported on TiO_2 have the maximum activity toward catalyzing CO oxidation.[4] Vajda et al. found that Pt8−Pt10 nanoclusters are highly active for oxidative dehydrogenation of propane.[5] Yoo et al. showed that Pt10−Pt15 nanoclusters supported on graphene have an unusually high activity for methanol oxidation reaction compared to Pt/carbon black catalyst.[6] These recent findings clearly indicate the importance of using small nanoclusters as innovative catalysts for various reactions. Nevertheless, the stability of nanoparticles in reaction conditions becomes a serious issue when their size is reduced to less than 5 nm.[7] Ultrasmall nanoclusters about 1 nm in diameter may easily deform into amorphous structures and become inactive under the influence of reactants.[8,9] Therefore, fundamental studies are needed to find ways for preventing NPs from reaction-driven deformation, coalescence, and also adsorption poisoning. One particularly promising approach is using bimetallic NPs.[10−16] Because of different atomic sizes and surface energies of two constituents, bimetallic NPs typically form well-defined core−shell structures in controlled synthesizing environments[17,18] and the core atoms may serve as anchors to withstand reaction-driven deformations. Furthermore, their electronic structure and catalytic activity can be tuned in a broad range by changing size, shape, and mixture of core and shell atoms. Whereas it is still difficult to access useful information regarding size and shape of NPs and the mutual influence between NPs and reactants through experimental means at this length scale, considerable insights can be established through computational simulations using the DFT. For example, comprehensive descriptions can be found in the literature for the core−shell preference in binary nanoparticle of late transition metals and noble metals.[18,19] Adsorption and reaction of small molecules such as CO on top of ultrasmall bimetallic clusters have also attracted attention.[20]

In this work, we study the M@Pt12 core−shell nanoclusters (less than 20 atoms), that is, with a transition metal M atom at the core and 12 Pt atoms on the shell, for the modification of reactivity and stability of the Pt13 nanoclusters. Clusters with 13 atoms have been studied intensively because they match the first magic number according to the geometric shell closing model with highly symmetric icosahedral (I_h) and cuboctaheral (Cubo-O_h) structures.[21−28] We found that the D_{5h} M@Pt12 (M = Fe, Co, Tc, Ru, Rh, Re, Os, or Ir) core−shell bimetallic nanoclusters

Received: January 31, 2012
Revised: May 28, 2012
Published: June 8, 2012

are highly resistive against the structural deformation and oxidation with the adsorption of oxygen. They also have lower adsorption energy of oxygen atoms compared to the pristine Pt13 nanocluster. Therefore, insertion of a suitable core atom is an effective way to make small Pt nanoclusters stable and catalytically active. This provides useful insights for the design of robust nanoparticles that are durable in actual reaction conditions.

2. MODEL AND CALCULATION

As shown in Figure.1, pure Pt13 and bimetallic M@Pt12 nanoclusters may adopt three symmetric structures, with the D_{5h},

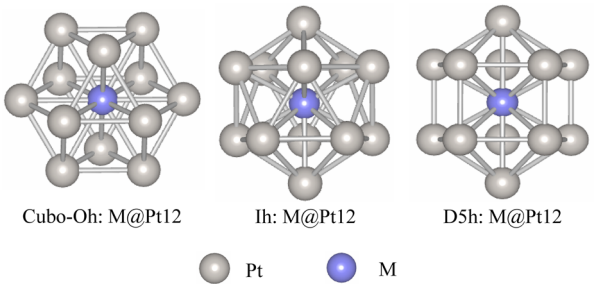

Figure 1. (Color online) Schematic models of the M@Pt12 structures considered.

Cubo-O_h, and I_h symmetries. Spin-polarized calculations are performed with the Vienna Ab-Initio Simulation Package (VASP).[29,30] The 3d4s shells of 3d atoms (Mn, Fe, Co, Ni, Cu), 4d5s shells of 4d atoms (Tc, Ru, Rh, Pd, Ag), and 5d6s shells of 5d atoms (Re, Os, Ir, Pt, Au), as well as 2s2p shells of oxygen atom are treated as valence states, whereas the ionic cores are represented by the projector augmented wave (PAW) potentials.[31] The Kohn–Sham orbitals are expanded using plane waves with a well-converged cutoff energy of 400 eV. The cluster is placed in a 15 × 15 × 15 Å^3 cubic supercell, which ensures at least 9 Å separation between the edges of adjacent periodic images. Only the gamma point in the tiny Brillouin zone (BZ) is used for cluster calculations, whereas a Monkhorst-Pack grid[32] of 11 × 11 × 11 Å^3 is used for the reference bulk metals. The exchange and correlation interactions among electrons are described at the level of the generalized gradient approximation (GGA) using the Perdew–Burke–Ernzerhof (PBE) formula.[33] The Gaussian smearing[34] method with a half-width of 0.05 eV is employed to accelerate convergence of charge and spin densities. To relax positions of atoms, we require energies and forces to converge better than 1.0 × 10^{-5} eV/atom and 0.01 eV/Å, respectively. The optimized lattice constant of bulk Pt is 3.95 Å, in good agreement with the measured value of 3.92 Å.[35] The bond length of a gas-phase O_2 molecule is 1.24 Å also very close to the experimental value of 1.21 Å.

3. RESULTS AND DISCUSSION

3.1. Stability of the Core–Shell M@Pt12 Particles. The structural stability of different clusters is characterized by three quantities. First, the relative stability of isomers is described by their cohesive energies defined as

$$E_{coh} = \sum_i E_i - E_{cluster} \quad (1)$$

where $E_{cluster}$ represents the total energy of a cluster and E_i represent energies of its constituent atoms, respectively. To reflect the benefit of substituting the central Pt atom with other element, we also define the change of cohesive energy

$$\Delta E_{coh} = E_{coh}(M@Pt12) - E_{coh}(Pt13) \quad (2)$$

For bimetallic surfaces, elements with lower surface energies generally tend to take surface sites. However, as the size of NPs decreases to 1 nm in diameter, this tendency may change due to various factors such as the quantum confinement effect and the change of bonding features. We thus also examine Pt@Pt11 M structures, that is, by swapping a surface Pt atom with the M atom in M@Pt12, and describe the site preference with the segregation energy of M,

$$E_{seg} = E_{Pt@Pt11M} - E_{M@Pt12} \quad (3)$$

From results collected in Table 1, one can see that the D_{5h} isomer is the most stable structure for the pure Pt13 cluster, in agreement with results of Aprà and Fortunelli.[36] Our total energies of Pt13 in the Cubo-O_h and I_h structures (−54.13, −53.92 eV) are also very close to results (−54.08, −53.87 eV) reported by Wang and Johnson.[25] Substitution of Cu, Pd, Ag, or Au for Pt at the core leads to reduction of cohesive energies, and they are thus unlikely to occur. These elements have negative E_{seg} (except for the I_h and D_{5h} Cu@Pt12), so they actually prefer surface sites. On the contrary, other transition metal elements have positive E_{seg} and thus they form stable M@Pt12 core–shell clusters. For most M@Pt12 isomers, the I_h and D_{5h} are close in energy, whereas the Cubo-O_h configuration is much less favored. Furthermore, the preference of the D_{5h} structure over the I_h structure for clusters with 3d core atoms (except for Co) is not as obvious as for those with 4d, 5d core atoms. Because the I_h structure is more compact than the D_{5h} structure, it allows the smaller 3d atoms to better interact with Pt atoms. In contrast, larger 4d and 5d atoms cannot be hosted in the I_h structure without pushing Pt atoms apart. Figure 2 shows a clear correlation between the radii of core atoms and the energy differences between the D_{5h} and I_h isomers. The preference of the D_{5h} structure is obvious for large core atoms in M@Pt12, supporting our conjecture.

For cases with $\Delta E_{coh} > 0$ in Table 1, the presence of core atoms strengthens the Pt12 cage, in comparison to the pristine D_{5h}-Pt13 cluster. It appears that core atoms in the left side of Pt in the periodic table (e.g., Mn, Fe, Co, Tc, Rh, Ru, Re, Os, Ir) lead to higher stability. On the contrary, elements in the right side of Pt (e.g., Cu, Ag, Au) lead to lower stability and they are more likely to form Pt@Pt11 M structures. This is understandable because these atoms have filled d-shells and they interact with their Pt neighbors without strong bonds. This argument also applies for Pd cases because the isolated Pd atom has a full d-shell.

Because D_{5h} M@Pt12 clusters are stable for most core atoms, we now focus on them to further illustrate the mechanism of core-induced stability enhancement. To better appreciate the qualitative trends, we summarize key results in Figure 3. In panel (a), one may see that E_{coh} of D_{5h} M@Pt12 clusters decreases as the number of d-electrons of the core atom increases. Therefore, the bonds formed between the core atom and Pt cage through d-band hybridization is the most crucial factor for the stability of the M@Pt12 clusters. In addition, as seen in part b of Figure 3, all stable D_{5h} M@Pt12 cluster have core atoms smaller than Pt, which somewhat tightens the Pt–Pt bonds in the shell. To confirm this point, we calculate energies of different D_{5h} M@Pt12 clusters with a frozen D_{5h} Pt13 structure. The corresponding data, as shown in the parentheses of Table 1

dx.doi.org/10.1021/jp300971e | J. Phys. Chem. C 2012, 116, 13774–13780

Table 1. Change of Cohesive Energy (ΔE_{coh}), and Segregation Energies (E_{seg}) of the M@Pt12 Clusters with Different Symmetry (M Represents the Late 3d, 4d, and 5d Transition-Metal Atoms), As Well As Data for the Pure Pt13 Cluster[a]

cluster	symmetry	E_{coh} (eV)	ΔE_{coh} (eV)	E_{seg1} (eV)	E_{seg2}(eV)	E_{seg} (eV)[18]
Pt@Pt12	I_h	46.46 46.29[35]	0.00	0		
	Cubo-O_h	46.60 43.03[35]	0.00	0		0
	D_{5h}	46.89 43.81[35]	0.00	0	0	
M for 3d						
Mn@Pt12	I_h	48.21	1.82	1.49		
	Cubo-O_h	47.53	1.04	0.34		X
	D_{5h}	48.11 (47.96)	1.18	1.41	1.08	
Fe@Pt12	I_h	49.10	2.71	1.75		
	Cubo-O_h	48.32	1.76	0.51		0.82
	D_{5h}	49.11 (48.84)	2.18	3.01 (2.40)	[b]	
Co@Pt12	I_h	48.38	1.82	1.26		
	Cubo-O_h	47.33	1.26	0.64		0.94
	D_{5h}	48.60 (48.16)	1.70	1.47	1.20	
Ni@Pt12	I_h	47.56	1.20	1.22		
	Cubo-O_h	47.02	0.37	0.37		0.42
	D_{5h}	47.46 (47.21)	0.59	0.88	0.72	
Cu@Pt12	I_h	46.35	−0.12	0.74		
	Cubo-O_h	45.7	−0.86	−0.45		−0.24
	D_{5h}	46.32 (46.18)	−0.55	0.52	0.52	
M for 4d						
Tc@Pt12	I_h	50.44	4.06	2.41		
	Cubo-O_h	50.00	3.42	1.70		X
	D_{5h}	50.67 (50.53)	3.78	2.49 (0.91)	[b]	
Ru@Pt12	I_h	49.40	3.00	1.60		
	Cubo-O_h	49.00	2.45	1.05		1.76
	D_{5h}	49.52 (49.45)	2.64	1.89	1.33	
Rh@Pt12	I_h	47.62	1.17	0.65		
	Cubo-O_h	47.51	0.94	0.00		0.75
	D_{5h}	47.92 (47.90)	1.03	0.73	0.67	
Pd@Pt12	I_h	44.89	−1.47	−0.44		
	Cubo-O_h	45.01	−1.65	−1.26		−0.44
	D_{5h}	45.28 (45.27)	−1.60	−0.61	−0.47	
Ag@Pt12	I_h	43.14	−3.25	−1.70		
	Cubo-O_h	43.24	−3.34	[b]		−1.99
	D_{5h}	43.61 (43.60)	−3.24	−1.34	[b]	
M for 5d						
Re@Pt12	I_h	53.69	5.27	[b]		
	Cubo-O_h	53.24	4.57	2.84		X
	D_{5h}	53.85 (53.70)	4.92	[b]	[b]	
Os@Pt12	I_h	50.81	4.36	2.34		
	Cubo-O_h	50.30	3.70	1.82		2.52
	D_{5h}	50.93 (50.86)	4.06	2.84 (0.61)	[b]	
Ir@Pt12	I_h	49.18	2.81	1.45		
	Cubo-O_h	48.98	2.42	1.06		1.48
	D_{5h}	49.41 (49.40)	2.55	1.58	1.22	
Au@Pt12	I_h	43.21	−3.22	−1.66		
	Cubo-O_h	43.47	−3.12	−1.79		−1.77
	D_{5h}	43.72 (43.71)	−3.11	−1.37	−1.46	

[a]For the D_{5h} structure, there are two nonequivalent Pt sites in the shell, so we considered E_{seg1} (eV) and E_{seg2} (eV) as segregation energies for the structures. The segregation energies from ref 18 are also shown for comparison. The numbers in parentheses are the calculated values for fixed D_{5h}-Pt13 atomic configurations in the column of E_{coh} (eV) and segregation energies of M@Pt12 clusters with an O adatom in the column of E_{seg1} (eV). [b]Refers to the structures are destroyed due to geometrical change. X means that the cases of Mn, Tc, Re are not included in the ref 18.

and also dashed lines in Figure 3, suggest that the atomic relaxation enhances E_{coh}, especially for clusters with 3d cores.

Charge transfers between atoms are determined through the Bader charge analysis scheme[37] and the Bader charges of core atoms are plotted in part c of Figure 3. Here, positive Bader charge corresponds to depletion of electrons from the core atom to Pt. In general, all core atoms lose electrons to the outmost Pt atoms that spill out their electrons to the vacuum region. Interestingly, E_{coh} scales with the Bader charge in part c of Figure 3, with an exception of Mn@Pt12. Because most charge depletion is from the s-shell of the core atom, the redistribution of s-electrons to the outmost surface also contributes to the

dx.doi.org/10.1021/jp300971e | J. Phys. Chem. C 2012, 116, 13774−13780

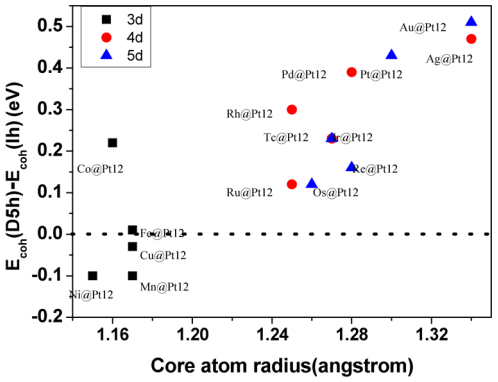

Figure 2. (Color online) Relationship of core atom radius and the cohesive energy difference between the D_{5h} and the I_h M@Pt12 isomers.

stability of cluster. This develops Coulomb attraction between the core and shell, and also fills the s-type molecular orbitals of the entire cluster, and both are beneficial for stabilizing the nanostructure. Note that the number of charge depletion in part c of Figure 3 can be somewhat predicted from the electronegativity.

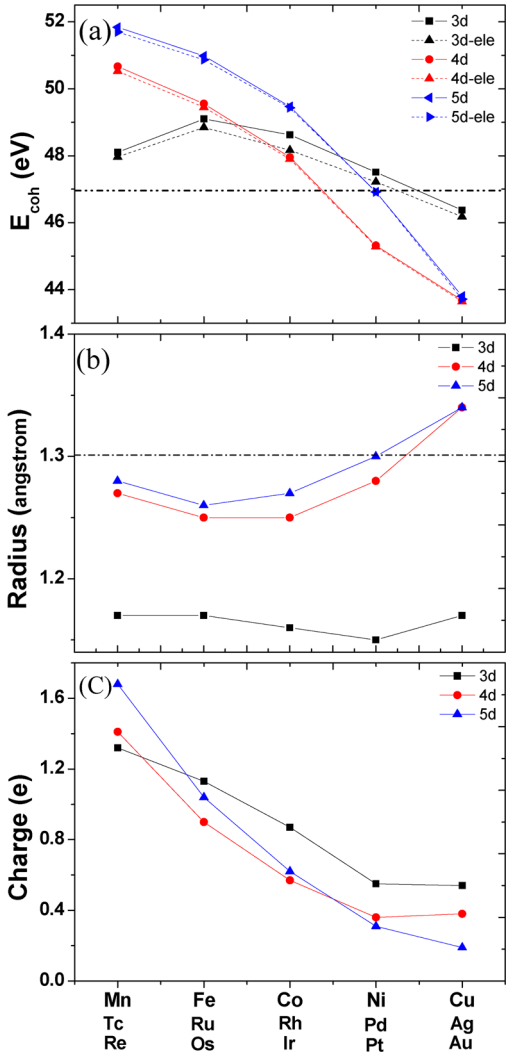

Figure 3. (Color online) Properties of the M@Pt12 and the M atoms: (a) the cohesive energies in solid line and the electronic cohesive energies in dash line, (b) the covalent radii of the M atoms, (c) the number of electrons lost by the M atom at the core.

3.2. Chemical Properties of the Pure D_{5h}-Pt13 Cluster.

Because the catalytic activity is closely related to electronic properties of surface atoms, we first analyze results of the density of states (DOS) and d-band centers of the D_{5h}-Pt13 cluster. It has 10 triangular (111) facets and 5 rectangular (100) facets, with Pt−Pt bonds of 2.62 and 2.71 Å, respectively. There are 2 nonequivalent atoms in the shell of the D_{5h}-Pt13 cluster, denoted as A (only in the 111 facets) and B (at corners of the 111 and 100 facets) in Figure 4. The DOS curves of the Pt13 cluster are

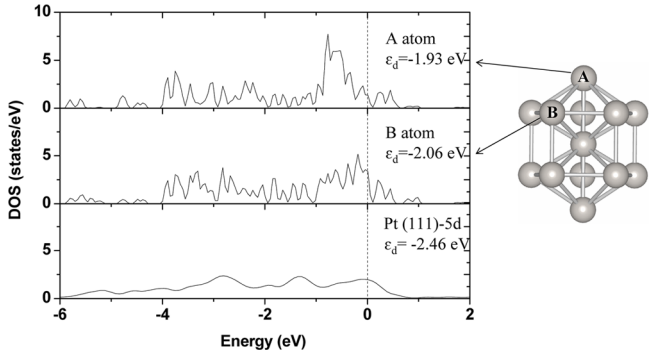

Figure 4. Surface d-band density of states (d-DOS) for the D_{5h}-Pt13 and the flat Pt(1 1 1) and the corresponding values of the d-band center (ε_d). The vertical broken line represents the Fermi energy.

obviously narrower than that of Pt(111) surface and the d-band center is also closer to the Fermi energy (E_F) than that of Pt (111). This is mainly because of the reduction in the coordination numbers in the Pt cluster, that is, 6 for A, 5 for B versus 9 for Pt (1 1 1). As known in the literature,[38] high DOS around E_F and a more shallow d-band center of transition metals correspond to high chemical activity. Quantitatively, the D_{5h}-Pt13 cluster has d-band centers at −1.92 eV (for A) and −2.06 eV (for B), substantially higher that of −2.46 eV for Pt (111).

To directly examine the catalytic activity of the D_{5h}-Pt13 cluster, we investigate the adsorption of an O_2 molecule, starting from seven initial symmetric configurations as shown in Figure 5.

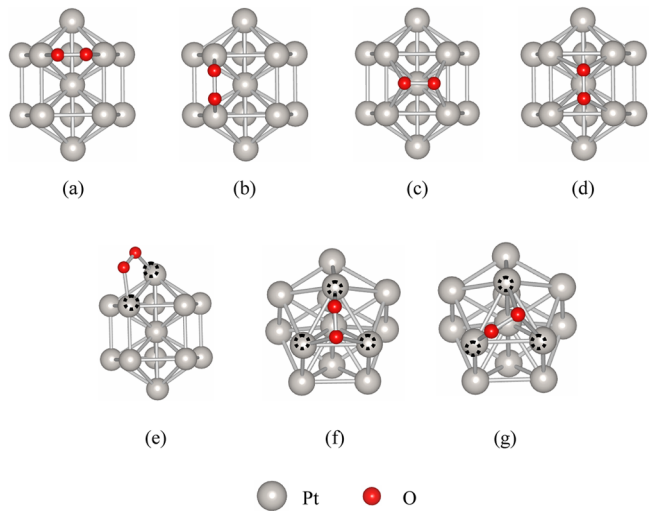

Figure 5. (Color online) Seven symmetric adsorption sites for O_2 on the D_{5h}-Pt13 cluster. The Pt atoms with the black dotted circles represent the Pt atoms on which the O_2 adsorbed.

dx.doi.org/10.1021/jp300971e | J. Phys. Chem. C 2012, 116, 13774−13780

After the structural optimization procedure without any constraint on symmetry, these configurations evolve to those in Figure 6 and their corresponding adsorption energies and O−O bond lengths are summarized right under them. Here, the adsorption energy of an O_2 molecule is defined by

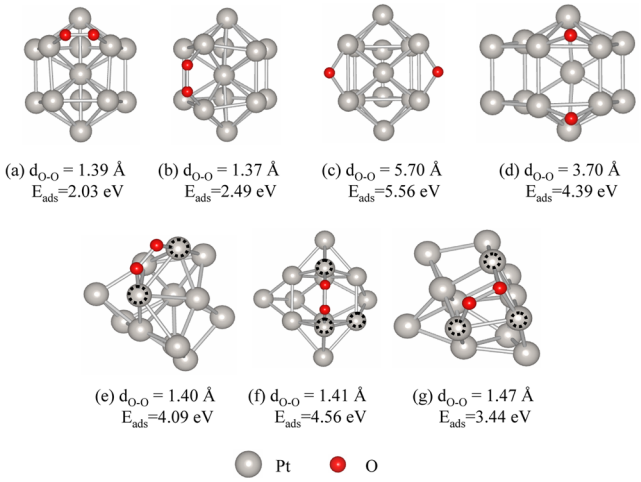

Figure 6. (Color online) Optimized structures for the adsorption of O_2 on the D_{5h}-Pt13 cluster at the seven symmetric O_2 adsorption sites selected.

$$E_{ads} = E_{O_2} + E_{cluster} - E_{O_2/cluster} \quad (4)$$

where E_{O_2} is the energy of an O_2 molecule in its gas-phase; $E_{O_2/cluster}$ and $E_{cluster}$ are the total energies of the cluster with and without O_2, respectively. The O_2 molecule is apparently activated on sites *a*, *b*, *e*, *f*, and *g* as manifested by the stretched O−O bond lengths (d_{O-O}, to 1.37−1.47 Å) and high adsorption energies (2.03−4.54 eV). Dramatically, O_2 even directly dissociates to two oxygen atoms on the *c* or *d* site. The O−O separation becomes as large as 5.70 or 3.70 Å and the adsorption energies for these atomic adsorption geometries are very large, up to 5.75 and 4.43 eV, respectively. Overall, O_2 binds to Pt13 cluster very tightly, in either molecular or atomic form, indicating that Pt13 cluster is indeed much more active than the flat Pt (111) surface, on which the adsorption energies of O_2 are about 0.45−0.63 eV and the corresponding O−O separations are around 1.36−1.40 Å.[39] Nevertheless, the Pt cluster is very vulnerable toward adsorbates. The minimum Pt−Pt bond expansion near O_2 is more than 10%. The Pt13 cluster even changes to amorphous form for cases with O_2 sitting on the *e*, *f*, and *g* sites. This indicates that, whereas pure Pt13 cluster can efficiently cleave O−O bonds, they may strongly deform and form local metal-oxide in view that O atoms bind so tightly to their Pt neighbors. This quickly degrades the catalytic performance of Pt13 in real reaction conditions.

3.3. Chemical Properties of M@Pt12 Core−Shell Clusters. Now we discuss adsorption of O_2 on several highly stable M@Pt12 clusters with M = Re, Tc, Fe, that may have practical use in fuel cells. Oxygen stays in the molecular form on the (111) facets, with the O−O bond expanding to 1.38−1.41 Å. However, adsorption energies of O_2 on the (111) facets are smaller by about 1.0 eV than those on the (100) facets and thus oxygen molecules should only take the (100) facets on these M@Pt12 clusters. To test if the stable M@Pt12 core−shell clusters are more robust than that Pt13 in real reaction conditions, we study two initial adsorption structures of O_2 as shown in parts a and a′ of Figure 7 corresponding to configuration *c* and *d* in Figures 5 and 6. Their optimized adsorption geometries

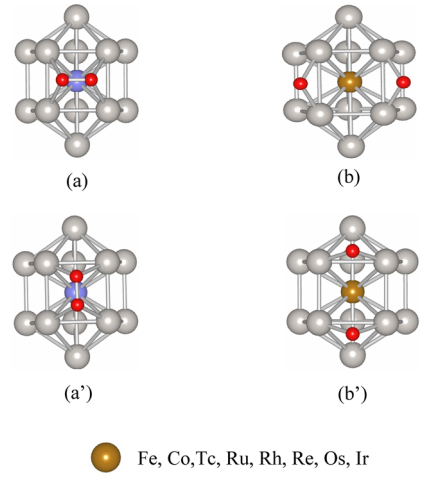

Figure 7. (Color online) (a) and (a′) Two initial adsorption sites selected for the O_2 on the D_{5h}-M@Pt12 cluster, and (b) and (b′) the final structures of a O_2 molecule dissociated on the *c* and *d* sites which retain the D_{5h} symmetry for the adsorption of an oxygen molecule on both the *c* and *d* sites.

displayed in parts b and b′ Figure 7 indicate that O_2 dissociates on these bimetallic clusters; the high activity of the Pt13 cluster is maintained well. Importantly, clusters with Fe, Co, Tc, Ru, Rh, Re, Os, or Ir atom at the core retain their D_{5h} symmetry well with the presence of oxygen molecules and adatoms, and thus they should be able to survive in reaction conditions. In the opposite side, adsorption of O_2 on other M@Pt12 NPs (M = Mn, Ni, Cu, Pd, Ag, Au) induces substantial structural changes away from the D_{5h} structure. From our results, good bimetallic nanocatalysts should have core atoms that provide large ΔE_{coh} and E_{seg}.

We know that catalytic activity results from a balance between low activation energies and rapid release of products. It was observed in experiments that small Pt clusters may dissociate O_2 more readily but they overbind oxygen atoms, which poisons the reaction cycle and hence reduces the activity of NPs as compared with the Pt(111) surface.[40] Recently, Adzic's work[41] showed a new route to achieve high ORR activity and durability of Pt−Ni nanocatalysts by using the hollow-induced lattice contraction, in order to decrease the adsorption energies of oxygen atoms. To further investigate the fittest D_{5h} M@Pt12 (M = Fe, Co, Tc, Ru, Rh, Re, Os, or Ir) nanoparticles as catalysts, we compare the adsorption energies of one oxygen atom ($E_{O,ad}$, half of the value as defined in eq 4). Table 2 shows the calculated adsorption energies of oxygen adatoms on different M@Pt12 clusters. In general, $E_{O,ad}$ lies in a range of 1.86−2.07 eV for the *c* configuration, and 1.49−1.61 eV for the *d* configuration. These values are already much lower than those (2.78, 2.21 eV) on the D_{5h}-Pt13 cluster. We stress that the overbinding of oxygen atom on the D_{5h}-Pt13 cluster mostly results from the large adsorption-induced structural change forming some local metal-oxide complexes. If we freeze the structure of the D_{5h}-Pt13 cluster and only allow O_2 to relax, O_2 also directly dissociates into two atoms in the *c* and *d* configurations, but $E_{O,ad}$ drastically reduces to 1.60 and 1.50 eV, respectively. Therefore, a proper core atom not only stabilizes the structure of the D_{5h} M@Pt12 clusters as compared with the pure D_{5h}-Pt13 cluster but also improves the reaction dynamics. The values of $E_{O,ad}$ on the D_{5h} M@Pt12

dx.doi.org/10.1021/jp300971e | J. Phys. Chem. C 2012, 116, 13774−13780

Table 2. Calculated Adsorption Energies of Oxygen Atoms on the D_{5h} M@Pt12 Cluster, the Values in Parentheses Are Calculated for the Fixed D_{5h}-Pt13 Cluster

system	adsorption site	$E_{O,ad}$(eV)	$d_{o\text{-}o}$(Å)	$d_{o\text{-}pt}$ (Å)
D_{5h}-Fe@Pt12	*c*	2.07	4.15	1.94
	d	1.52	3.51	1.95
D_{5h}-Co@Pt12	*c*	2.03	4.17	1.94
	d	1.50	3.48	1.95
D_{5h}-Tc@Pt12	*c*	1.91	4.27	1.94
	d	1.54	3.39	1.95
D_{5h}-Ru@Pt12	*c*	1.91	4.21	1.94
	d	1.53	3.47	1.95
D_{5h}-Rh@Pt12	*c*	1.97	4.20	1.94
	d	1.61	3.54	1.95
D_{5h}-Re@Pt12	*c*	1.89	4.30	1.94
	d	1.54	3.38	1.96
D_{5h}-Os@Pt12	*c*	1.86	4.23	1.94
	d	1.54	3.42	1.96
D_{5h}-Ir@Pt12	*c*	1.89	4.15	1.94
	d	1.56	3.52	1.95
D_{5h}-Pt13	*c*	2.78(1.62)	5.70(4.35)	1.96(1.93)
	d	2.21(1.50)	3.70(3.53)	1.95(1.94)

clusters are actually comparable to that (1.93 eV) of an oxygen atom on the Pt(111) surface at low coverage.[17]

Finally, we want to discuss if the active core atoms may get pulled out to the shell by the oxygen adatoms. As listed in Table 1, for several M@Pt12 and Pt@Pt11 M clusters (with M = Fe, Tc, and Os, which possess the biggest M−O binding energies for the 3d, 4d, 5d metals we selected), we found that indeed, the values of E_{seg} with an O atom adsorption at the most favorable site (the top site of M atom on the Pt@Pt11 M clusters or one of the Pt−Pt bridge sites on the M@Pt12 as shown in part b of Figure 7) decreased compared to those without O atom adsorption. However, the values of E_{seg} keep positive for all the tested cases, which show that our selected M@Pt12 core−shell clusters are stable even with the O atom adsorption.

CONCLUSIONS

To shed some light for the search of effective bimetallic nanocatalysts for ORR in fuel cells, we systematically studied the structural stability and reactivity of pure and alloyed Pt13 clusters through density functional calculations. Oxygen molecules may directly dissociate on the (100) facets of these clusters so the stability of their own structures is the main concern for the durability in applications. We found that good core atoms should provide large ΔE_{coh}, and E_{seg} or, more fundamentally, with low electronegativity and the substitution of Fe, Co, Tc, Ru, Rh, Re, Os, or Ir in its core, forming D_{5h} M@Pt12 core−shell, significantly enhances the structural stability and also further improves its catalytic activity. Our findings provide useful insights for the design of robust bimetallic nanocatalysts.

AUTHOR INFORMATION

Corresponding Author

*E-mail: yzx@henannu.edu.cn (Z.Y.), wur@uci.edu (R.W.).

Notes

The authors declare no competing financial interest.

ACKNOWLEDGMENTS

This work was supported by the National Natural Science Foundation of China (Grant No. 11174070) and the Innovation Scientists and Technicians Troop Construction Projects of Henan Province, China (Grant No. 104200510014). Work at UCI was supported by DOE grant DE-FG02-05ER46237 and computing time on supercomputers at NERSC.

REFERENCES

(1) Whitesides, G. M.; Crabtree, G. W. *Science* **2007**, *315*, 796−798.
(2) T. R. Ralph, M. P. H. *Platin. Met. Rev.* **2001**, *46*, 1−4.
(3) Baletto, F.; Ferrando, R. *Rev. Mod. Phys.* **2005**, *77*, 371−423.
(4) Kaden, W. E.; Wu, T.; Kunkel, W. A.; Anderson, S. L. *Science* **2009**, *326*, 826−829.
(5) Vajda, S.; Pellin, M. J.; Greeley, J. P.; Marshall, C. L.; Curtiss, L. A.; Ballentine, G. A.; Elam, J. W.; Catillon-Mucherie, S.; Redfern, P. C.; Mehmood, F.; et al. *Nat. Mater.* **2009**, *8*, 213−216.
(6) Yoo, E.; Okata, T.; Akita, T.; Kohyama, M.; Nakamura, J.; Honma, I. *Nano Lett.* **2009**, *9*, 2255−2259.
(7) Sasaki, K.; Naohara, H.; Cai, Y.; Choi, Y. M.; Liu, P.; Vukmirovic, M. B.; Wang, J. X.; Adzic, R. R. *Angew. Chem., Int. Ed.* **2010**, *49*, 8602−8607.
(8) Kim, H. Y.; Kim, D. H.; Ryu, J. H.; Lee, H. M. *J. Phys. Chem. C* **2009**, *113*, 15559−15564.
(9) Sun, Y.; Zhuang, L.; Lu, J.; Hong, X.; Liu, P. *J. Am. Chem. Soc.* **2007**, *129*, 15465−15467.
(10) Kim, H. Y.; Kim, H. G.; Ryu, J. H.; Lee, H. M. *Phys. Rev. B.* **2007**, *75*, 212105.
(11) Kim, H. Y.; Kim, H. G.; Kim, D. H.; Lee, H. M. *J. Phys. Chem. C* **2008**, *112*, 17138−17142.
(12) Ferrando, R.; Jellinek, J.; Johnston, R. L. *Chem. Rev.* **2008**, *108*, 845−910.
(13) Gao, Y.; Shao, N.; Bulusu, S.; Zeng, X. C. *J. Phys. Chem. C* **2008**, *112*, 8234−8238.
(14) Pyykkö, P.; Runeberg, N. *Angew. Chem., Int. Ed.* **2002**, *41*, 2174−2176.
(15) Yang, Z.; Zhang, Y.; Wang, J.; Ma, S. *Phys. Lett. A* **2011**, *375*, 3142−3148.
(16) Kim, H. Y.; Han, S. S.; Ryu, J. H.; Lee, H. M. *J. Phys. Chem. C* **2010**, *114*, 3156−3160.
(17) Froemming, N. S.; Henkelman, G. *J. Chem. Phys.* **2009**, *131*, 234103−234109.
(18) Wang, L.-L.; Johnson, D. D. *J. Am. Chem. Soc.* **2009**, *131*, 14023−14029.
(19) Yuan, D. W.; Gong, X. G.; Wu, R. Q. *Phys. Rev. B* **2008**, *78*, 035441−035444.
(20) Morrow, B. H.; Resasco, D. E.; Striolo, A.; Nardelli, M. B. *J. Phys. Chem. C* **2011**, *115*, 5637−5647.
(21) Kumar, V.; Kawazoe, Y. *Phys. Rev. B* **2002**, *65*, 125403−125413.
(22) Longo, R. C.; Gallego, L. J. *Phys. Rev. B* **2006**, *74*, 193409−193413.
(23) Moseler, M.; Häkkinen, H.; Barnett, R. N.; Landman, U. *Phys. Rev. Lett.* **2001**, *86*, 2545−2548.
(24) Akola, J.; Häkkinen, H.; Manninen, M. *Phys. Rev. B* **1998**, *58*, 3601−3604.
(25) Wang, L. L.; Johnson, D. D. *Phys. Rev. B* **2007**, *75*, 235405−235414.
(26) Pal, R.; Cui, L. F.; Bulusu, S.; Zhai, H. J.; Wang, L. S.; Zeng, X. C. *J. Chem. Phys.* **2008**, *128*, 024305−024312.
(27) Li, S. F.; Gong, X. G. *Phys. Rev. B* **2006**, *74*, 045432.
(28) Femoni, C.; Iapalucci, M. C.; Longoni, G.; Zacchini, S.; Zarra, S. *J. Am. Chem. Soc.* **2011**, *133*, 2406−2409.
(29) Kresse, G.; Furthmüller, J. *Comput. Mater. Sci.* **1996**, *6*, 15−50.
(30) Kresse, G.; Furthmüller, J. *Phys. Rev. B* **1996**, *54*, 11169−11186.
(31) Kresse, G.; Joubert, D. *Phys. Rev. B* **1999**, *59*, 1758−1775.
(32) Monkhorst, H. J.; Pack, J. D. *Phys. Rev. B* **1976**, *13*, 5188−5192.
(33) Perdew, J. P.; Burke, K.; Ernzerhof, M. *Phys. Rev. Lett.* **1996**, *77*, 3865−3868.
(34) Methfessel, M.; Paxton, A. *Phys. Rev. B* **1989**, *40*, 3616−3621.
(35) Branger, V.; Pelosin, V.; Badawi, K.; Goudeau, P. *Thin Solid Films* **1996**, *275*, 22−24.

(36) Aprà, E.; Fortunelli, A. *J. Phys. Chem. A* **2003**, *107*, 2934−2942.
(37) Henkelman, G.; Arnaldsson, A.; Jónsson, H. *Comput. Mater. Sci.* **2006**, *36*, 354−360.
(38) Hammer, B.; Nørskov, J. K. *Adv. Catal.* **2000**, *45*, 71−129.
(39) Yang, Z.; Wang, J.; Yu, X. *Phys. Lett. A* **2010**, *374*, 4713−4717.
(40) Shao, M.; Peles, A.; Shoemaker, K. *Nano Lett.* **2011**, *11*, 3714−3719.
(41) Wang, J. X.; Ma, C.; Choi, Y.; Su, D.; Zhu, Y.; Liu, P.; Si, R.; Vukmirovic, M. B.; Zhang, Y.; Adzic, R. R. *J. Am. Chem. Soc.* **2011**, *133*, 13551−13557.